Resonant Raman scattering by CdTe quantum-well-confined optical phonons in a semiconductor microcavity

A. Bruchhausen* and A. Fainstein†
Instituto Balseiro & Centro Atómico Bariloche, C.N.E.A., R8402AGP Bariloche, RN, Argentina

B. Jusserand
Institut des Nanosciences de Paris, UMR CNRS 7588, Université Pierre et Marie Curie, Campus Boucicaut, 140 Rue de Lourmel, 75015 Paris, France

R. André
Laboratoire de Spectrométrie Physique, Université Joseph Fourier-Grenoble 1, CNRS, Boîte Postale 87, F-38402, St. Martin d'Heres Cedex, France

(Received 15 October 2005; published 6 February 2006)

We present a Raman scattering study of CdTe quantum well (QW) optical phonons in a II-VI semiconductor microcavity. These have been performed under outgoing resonance conditions with the cavity polaritons. The CdTe optical phonon spectra show a main peak and smaller oscillationlike features towards lower phonon energies, which are assigned to QW confined phonons. The fact that the oscillations are found to be equidistant, thus leading to an almost linear effective dispersion for the confined phonons, is attributed to segregation and interdiffusion of atoms at the QW interfaces providing a rather parabolic-shaped phonon-confining potential. An "effective-mass" model is used to describe the optical phonon confinement, leading to microscopic information on the compositional profile of the QW's embedded within the optical cavity.

DOI: 10.1103/PhysRevB.73.085305 PACS number(s): 78.30.Fs, 63.22.+m, 78.67.−n

I. INTRODUCTION AND MOTIVATION

Confinement of optical vibrations to individual layers of semiconductor heterostructures (such as superlattices, quantum wells, and slabs) is well known and has been extensively studied in the past.[1–11] The confinement occurs when the optical-mode frequencies of the constituent materials differ considerably, impeding the phonon propagation from one layered material to the next. If such is the case, the phonon momentum gets quantized along the epitaxial growth direction $\hat{z}$, normal to the layers, and is given within a perfectly confining model by[1,2]

$$q_z = \frac{\pi}{d+\Delta} m. \tag{1}$$

Here $m=1,2,3\ldots$ indicates the quantization order, d is the layer thickness, and Δ is the phenomenological parameter that relaxes the "rigid barrier" condition accounting for the optical vibration penetration into the neighboring layer. Usually, for zinc-blende-type materials epitaxially grown along the [001] direction, Δ is taken as one atomic layer.[1,11] For polar semiconductor heterostructures, in addition to this mechanical boundary condition the collective movement of the ionic layers has associated a macroscopic electric field. Because of these long-range quasielectrostatic forces, the optical phonon modes (especially the odd-confined modes) result of highly dispersive nature with increasing in-plane wave vector ($q_\parallel$).[2–5]

Raman scattering has been widely used to study these excitations, proving to be a powerful technique for that purpose.[1,2] Due to the symmetry of the electron- (exciton-) phonon interactions involved in the scattering processes, two different cases need to be distinguished.[8] For experiments performed far from electronic resonance (e.g., with the excitonic 1*s* state), scattering is mainly through deformation potential interaction and odd-order phonon modes dominate the Raman spectra in the back scattering ($q_\parallel=0$) configuration. In this case, the Raman shift due to the confined phonons plotted against their effective wave vector [given by Eq. (1)] map out the bulk dispersion.[1,2,11] If, on the other hand, the excitation energy is tuned near an electronic state, the situation turns out to be more complex. A Fröhlich interaction dominates over the deformation potential, and since the Fröhlich interaction has opposite symmetry from that of the deformation potential, even-order phonon modes produce a Raman-active contribution to the scattering strength for backscattering experiments.[8] In addition, due to the activation of elastic scattering mechanisms (impurity or roughness induced) at near-outgoing resonant excitation condition, relaxation of the wave-vector selection rules allows coupling with in-plane ($q_\parallel \neq 0$) modes.[2,8,9] Therefore the Raman outgoing line shape results from a mixture of the pure even-order confined phonon modes and those Raman-active modes with finite $q_\parallel$.[10,11]

The fact that optical phonons in heterostructures are strongly influenced by confinement has led to their use for the determination of the confinement potential and, through it, of the quantum well (QW) shape and interface quality.[7,12–14] These latter issues are a matter of great interest in the search for higher-quality thin QW's with controlled interfaces. In fact, the profiles of so-called normal and inverted interfaces have been studied in both III-V and II-VI materials through several techniques that include, besides Raman scattering, surface-sensitive techniques, x rays, and

magneto-optics.[12,15–17] Depending on the materials and the growth temperature, either or both of the intervening mechanisms (segregation and interdifusion) play a major role. Segregation produces approximately exponential profiles that are asymmetric relative to the growth direction.[7,14–17] Interdifussion, on the other hand, leads to symmetric Gaussian-like profiles.[13,18]

In the present paper we report results of first-order Raman scattering due to confined optical phonons of CdTe QW's embedded in an optical microcavity. This microcavity has been designed to show strong exciton–cavity-photon coupling.[19–21] The strong coupling leads to new mixed photon-exciton eigenstates denominated cavity-exciton polaritions. In the strong-coupling regime, Raman scattering due to phonons is not mediated by QW excitons, but by polaritons.[19,20] The process of Raman scattering mediated by polaritons was the subject of previous investigations.[21] These experiments were performed with the laser excitation tuned at outgoing resonance with one of the polariton branches of the cavity.[21] The added cavity and excitonic resonance involved in the polariton-mediated Raman process leads to strongly enhanced Raman efficiencies ($\sim 10^6$–10^7). In the present work, we will use such a strong enhancement to study the details of the phonon spectra in the CdTe QW's. Because of this cavity-polariton resonant enhancement, we have been able to observe confined phonons up to an order of $m=12$. Since the confined phonons are very sensitive to the local properties of the structure, they give information on the potential well in which they are confined.[6,7,13,14,22] Based on the effective phonon dispersion we analyze the composition profile of the QW's embedded within the optical microcavity.

II. SAMPLE AND EXPERIMENTAL DETAILS

The sample studied was grown by molecular beam epitaxy (MBE) and consists of three $d_1=72$ Å CdTe QW's, separated by $d_2=69$ Å $Cd_{0.4}Mg_{0.6}Te$ barriers, and embedded in a $\lambda/2$ $Cd_{0.4}Mg_{0.6}Te$ cavity spacer. The latter is enclosed by $Cd_{0.4}Mg_{0.6}Te/Cd_{0.75}Mn_{0.25}Te$ Bragg mirrors, with 21 mirrors pairs on the bottom and 15.5 pairs on the top. All layers constituting the sample were grown with a thickness gradient that enables the tuning of the cavity mode by displacing the spot over the sample. The experiments were performed in a backscattering $z(x,x')z'$ configuration, where z (z') and x (x') describe the incident (scattered) beam direction and polarization, respectively.[23] In our case, x and x' refer to the $\langle 110\rangle$ direction, z to the $\langle 001\rangle$ growth direction, and $z'\equiv\bar{z}$ (backscattering along $\langle 001\rangle$). A tunable cw Ti:sapphire laser was used at almost normal incidence with power ~ 50 μW and focalized to a spot of $\varnothing\sim 50$ μm. The collection cone normal to the sample surface was fixed at 3°, corresponding to an uncertainty in the in-plane wave vector of $k_{\parallel}\approx 4.2\times 10^3$ cm^{-1}. The working temperature was set at 2.3 K using a liquid-He cryostat. At this temperature, the sample shows a double anticrossing of the cavity mode with both the 1s and 2s exciton modes;[21] i.e., three polariton branches are present. Figure 1 shows the experimental polariton dispersion (circles) for the middle (MP) and lower (LP) branches, derived from photoluminescence spectra. The upper polariton branch (UP) was not observed with luminescence at this temperature. The solid lines are a fit to the data using a simple three-coupled-mode model, with Rabi splittings of $\Omega_{P\text{-}1s}\sim 13$ meV and $\Omega_{P\text{-}2s}\sim 5$ meV. The dashed and dash-dotted lines correspond to the bare (noninteracting) exciton (X_{1s} and X_{2s}) and cavity-photon (P) dispersions used in the model, respectively.[21] The small positive slope of the bare exciton dispersions is due to the thickness gradient, which also affects the QW's. All the results reported here were performed at *constant* cavity photon-exciton detuning (i.e., at a fixed spot position), tuned to match the first anticrossing, which is the minimum separation between the middle and lower polariton branches ($\Delta E_{MP\text{-}LP}\approx 13$ meV). The experiments were performed at outgoing resonance with the middle polariton branch, as indicated with the larger dot in Fig. 1. Similar data were obtained for other detunings. The spectra were analyzed using a Jobin-Yvon T64000 triple spectrometer in subtractive mode, equipped with a liquid-N_2-cooled charge-coupled device (CCD).

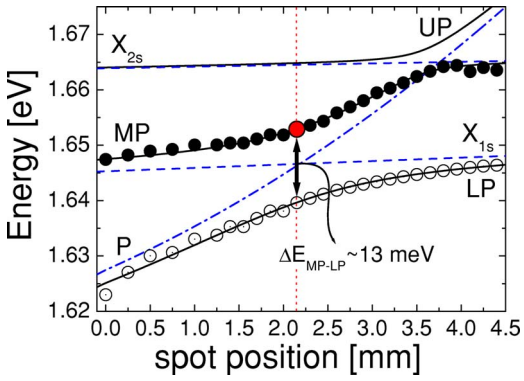

FIG. 1. (Color online) Polariton-mode energy as function of the position of the spot on the sample. The experimental data (circles) were derived from photoluminescence spectra and were fitted (solid lines) using a simple three-coupled-mode model (see text for details). The dashed and dash-dotted lines correspond to the bare exciton (X_{1s}, X_{2s}) and cavity-photon (P) dispersions, respectively. The dotted line indicates the position and photon-exciton detuning at which the reported results were performed. These were taken at outgoing resonance with the MP branch, as highlighted with a larger dot.

III. RESULTS AND DISCUSSION

Figure 2 shows a typical outgoing resonant Raman scan taken in the $z(x',x')\bar{z}$ configuration, in proximity to the middle polariton branch. The spectra correspond to first-order LO-phonon scattering. The scan was performed for varying laser energy at a fixed detuning ($\delta=0$) corresponding to exact anticrossing between the cavity mode and the 1s exciton. In the picture, the broad peak centered around 1.6532 eV, indicated with a vertical dotted line, corresponds to the middle polariton luminescence. On top of it, narrow peaks are observed that correspond to the Stoke-shifted photons due to the CdTe QW LO phonons. They shift with varying laser energy. The Raman spectra consist of a main peak, which becomes enhanced when tuned at exact outgoing reso-

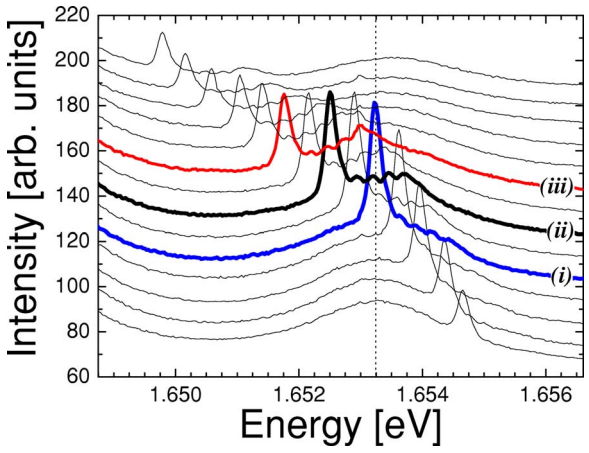

FIG. 2. (Color online) First-order LO-phonon Raman spectra taken at 2.3 K, for varying laser energy at outgoing resonance with the middle polariton mode. The Raman intensity resonates at the middle polariton energy, seen as a broad luminescence peak located around 1.6532 eV. Excitation energies for the bottom, at resonance, and top spectra are around 1.6761, 1.6747, and 1.6713 eV, respectively. Note in the spectra that, besides the main LO-phonon peak, small oscillations can be observed towards higher energies. The latter, assigned to the QW-confined LO phonons, also become more evident at resonance with the middle polariton.

nance with the middle polariton.[21] Some resonant spectra are highlighted in the figurewith thick solid lines. Besides the main LO peak, clear small almost equidistant oscillations towards higher energies (i.e., smaller Raman shift) are observed. These, as well as the main LO peak, become more intense when their energy coincides with the middle polariton.[21] As will be shown below, the oscillations are due to CdTe QW confined LO phonons. The tail observed at lower energies in Fig. 2 is due to luminescence coming from the lower polariton branch.[21]

For the purpose of a better analysis of the Raman spectra, the three selected spectra indicated with thick solid lines in Fig. 2, are plotted in Fig. 3 as function of the *Raman shift*. It is important to keep in mind that each spectra corresponds to

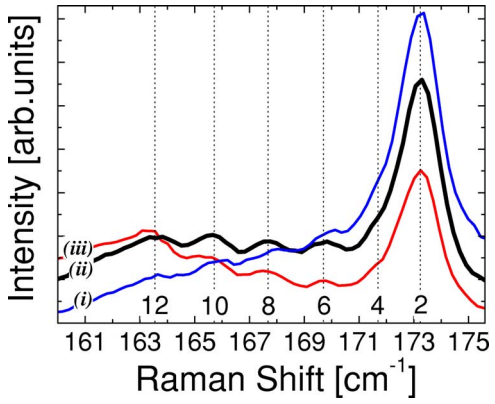

FIG. 3. (Color online) A close-up of the three Raman spectra indicated in Fig. 2 with thicker lines and labeled with the same indexes (i), (ii), and (iii), respectively. The vertical dotted lines indicate the even-confined phonon-mode order to which each maximum is assigned.

a different resonant condition, and therefore the intensity of the peaks, as well as the background due to the middle polariton luminescence, need not be the same. For spectrum (i) the main peak is tuned at exact resonance with the middle polariton, whereas (ii) and (iii) are detuned to lower absolute energies. In this close-up the Raman line shapes can be clearly observed. The main peak at 173.25 cm^{-1} is slightly asymmetric and displays a shoulder 1.41 cm^{-1} towards lower energies. The spectra display towards smaller Raman shifts the oscillations, with maxima 3.42, 5.51, 7.65, and 9.83 cm^{-1} downshifted from the main LO peak. These maxima are indicated in the figure, together with the main peak and the shoulder, by vertical dotted lines.

Since exciton polaritons interact with phonons only through their exciton component,[19–21] the same Raman selection rules as for pure exciton-mediated inelastic light scattering hold. As mentioned above, under resonant conditions the Raman scattering by LO phonons is mediated by the Fröhlich interaction. The established knowledge indicates that this leads, for the $z(x',x')\bar{z}$ scattering geometry used, to the observation of QW-confined phonons of even order.[8–11] A quantitative detailed description of the Raman line shape under outgoing resonance in GaAs QW's has been provided by Shields and co-workers.[11] When a full description of the Raman process is performed, it turns out that for the strong outgoing resonant case the Raman line shape does not correspond only to confined even modes of $q \sim 0$, but to a mixture of even-order confined modes and bands formed by the scattering due to strongly dispersive modes with finite in-plane wave vector. The latter become active due to roughness induced elastic scattering. These bands (due to so-called "interface" modes) display anticrossings with the odd-confined-mode energies.[5,10,11] At these anticrossings, dips in the scattered intensity arise, leading to maxima in between the odd modes—that is, to peaks close to the position of the even-order confined modes. Thus, both Fröhlich-allowed scattering and roughness-induced processes lead to peaks that, in a good approximation, correspond to the even-confined-mode position. Therefore we attribute the observed main Raman peak to scattering due to the first even-order confined CdTe phonon (LO_2) and assign the oscillation maxima to confined QW phonons of higher even order (LO_m, with m even).

In Fig. 4, the differences of each Raman oscillation maxima with the LO_2 peak ($\Delta\omega_{LO_2\text{-}LO_m}$ in cm^{-1}) is plotted as a function of the LO_2 Stokes energy (in eV) for all spectra in the scan of Fig. 2. Two main observations follow from this figure. First, the oscillation maximum separation with the LO_2 line is independent of the laser energy, thus unambiguously identifying these features with Raman signals. And second, the oscillations and the shoulder are almost equidistant. This follows from the horizontal lines in Fig. 4, which are fits to the experimental data with a constant value.[37] From these fits the separation $\Delta\omega_{LO_m\text{-}LO_{m+2}}$ equals 2.01, 2.09, 2.14, and 2.18 cm^{-1} for even m=4–10, respectively.

Figure 5 shows the experimental Raman shifts, derived from Fig. 4, plotted against the corresponding effective confinement order (open squares). Plotted in the same figure (solid squares) is the calculated dispersion for the confined

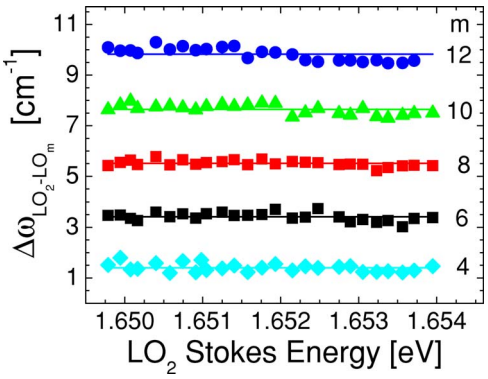

FIG. 4. (Color online) The frequency difference of the main peak (m=2, LO_2) and the other even confined modes (LO_m, m=4–12), as a function of the LO_2 Stokes energy, for the Raman scan with varying laser energy shown in Fig. 2. The solid lines are a constant fit to the experimental data.

phonons assuming the perfect confining or rigid barrier model described by Eq. (1). Note again the rather anomalous linearity of the experimental dispersion in contrast to the paraboliclike curve described by the simple model. As we discuss next, this will provide valuable information about the phonon confining potential—i.e., the compositional profile of the QW's inside the optical cavity.[6,7,22]

Detailed studies of the effect of QW shape on the phonon dispersion have been reported by different authors using both Raman and x-ray diffraction techniques in III-V-type semiconductor superlattices.[6,7,13,22] The observation of phonon dispersions that differ strongly with those corresponding to the "ideal square confining" potential has been interpreted as evidence that the studied QW's are indeed far from having abrupt interfaces and tend more to exponential-like asymmetric profiles, induced by segregation, or to parabolic shapes due to interdiffusion. To quantitatively derive the potential acting on the phonons on the studied CdTe QW's,

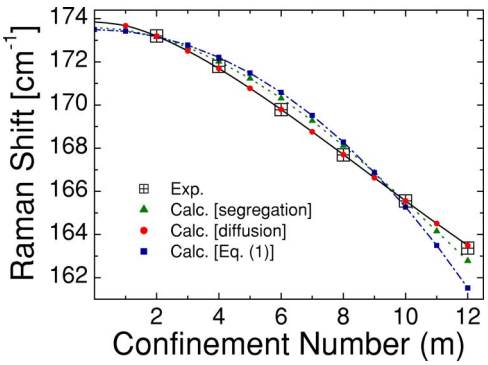

FIG. 5. (Color online) Comparison between the experimental (open squares) and calculated effective confined phonon dispersions. Triangles and solid circles correspond, respectively, to dispersions obtained for the proposed segregation and interdiffusion profiles. For completeness, the calculated confined phonon dispersion using the perfect confining rigid barrier model is also shown (solid squares). The dotted, solid, and dash-dotted lines are interpolations of the calculated results, respectively. Note the linearity of the experimental data.

calculations using a LO-phonon *effective-mass* model have been performed and will be described next.

IV. COMPARISON OF CALCULATIONS AND EXPERIMENT

We assume a phenomenological model valid for polar long-wave LO vibrations in semiconductors and based on a macroscopic continuum theory.[3,4] Neglecting electrostatic boundary conditions, under the assumption of in-plane translational symmetry and zero in-plane wave vector ($q_{\parallel}$=0), the equation for the longitudinal relative ionic displacement field $u(z)$ along the confinement direction is described by[3,4,13]

$$\left[\omega_{LO}^2 + \beta^2 \frac{d^2}{dz^2}\right] u(z) = \omega^2 u(z), \tag{2}$$

where the bulk LO frequency ω_{LO} and the velocity parameter β depend on the material. For binary alloys like $Cd_{1-X}Mg_XTe$, these parameters can be taken as functions of the atomic fraction X.

Since our interest is centered on the QW phonons, ω_{LO} corresponds to the bulk CdTe-like mode of the alloy at Γ ($\mathbf{q}$=0). The dependence of the mode frequencies on X is modeled as a simple linear expression, similar to that used in Ref. 13:

$$\omega_{LO}^2(X) = \omega_b^2(1 - \alpha X). \tag{3}$$

ω_b is the CdTe bulk frequency at Γ, and the parameter $\alpha \sim 0.26$ was obtained fitting the experimental data from Ref. 24. α is assumed as constant and sample independent, while ω_b will *a priori* be more susceptible to sample conditions (i.e., temperature, strain, confinement, etc.[25]) and is thus left as a fitting parameter ω_0 in our model. The dependence of the dispersion parameter β of the alloy CdTe-like mode with X is, to the best of our knowledge, not reported in the literature. We thus adopt a similar assumption as that made in Ref. 13 for GaAs: that is

$$\beta^2(X) = (1 - X)\beta_0^2, \tag{4}$$

where $\beta_0 \sim 2.33 \times 10^5$ cm/s is the CdTe-bulk dispersion parameter, which was obtained by fitting neutron-scattering data from Ref. 26 using a quadratic dispersion relation. The factor $(1-X)$ takes into account the fact that, for low Mg concentration, the CdTe-like LO phonon mode of the alloy tends to the CdTe-bulk dispersion.

Under these assumptions, the compositional profile of the sample can be represented by a variation of X with z [$X(z)$], taking values between zero for pure CdTe (QW material) and 0.6 for $Cd_{0.4}Mg_{0.6}Te$ (barrier material). Replacing Eqs. (3) and (4) in Eq. (2) leads to the "effective-mass" equation

$$\left[\omega_0^2(1 - \alpha X(z)) + (1 - X(z))\beta_0^2 \frac{d^2}{dz^2}\right] u(z) = \omega^2 u(z). \tag{5}$$

The square root of the first term on the left-hand side describes the energy of the CdTe-like optical phonons as a function of composition (consequently of z) and plays the role of a phonon-confining potential. The eigenvalues of Eq.

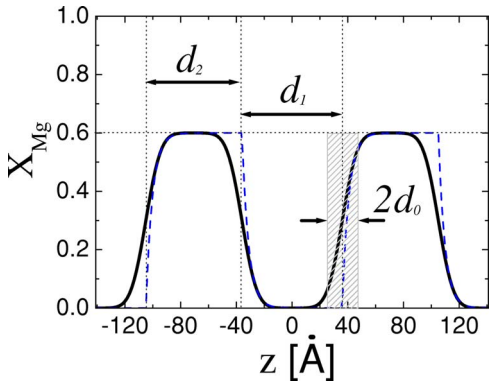

FIG. 6. (Color online) Sketch of the compositional profiles of one of the three QW's used in our effective-mass model. d_1 =72 Å and d_2=69 Å indicate the nominal QW and barrier widths, respectively. The dashed line corresponds to the segregation profile and the solid line to the proposed interdiffusion profile. d_0 is the transition (interface) width, which turned out to be of about 11 Å.

(5) represent the confined phonon energies ω_m, and the eigenvectors correspond to the vibrational normal modes $u_m(z)$ of the structure.

To solve Eq. (5), two interface profiles were used corresponding to different interface-intermixing mechanisms: namely, a discrete quasiexponential one, related to segregation, and a continuous error function profile, linked to interdiffusion. The segregation-induced profile was calculated assuming that exchange of Mg and Cd takes place only between the layer being grown and the one immediately below. For this purpose we used the mass action law, which relates the magnesium atomic fraction x at the last layer that is being grown (x_s) to that of the first underlying layer (x_b) by the relation $x_b(1-x_s)/x_s(1-x_b)=C=\exp(E_s/k_BT)$.[15,17] Here T is the growth temperature, k_B is the Boltzmann constant, E_s is a phenomenological segregation energy, and the process is recursively repeated to determine the concentration of all layers.[12,14–17] For Mn and Cd exchange it has been experimentally determined that $C\sim 1$.[16,17] We are not aware of similar data reported for Mg, and thus we have assumed the same value in our calculations. The resulting profile is shown in Fig. 6 (dashed line). It is worth mentioning that the segregation process (within this model) depends only on the thermodynamic (chemical) equilibrium between the two involved layers (the surface and first underlying one). Once the parameter E_s is fixed by the materials involved, the profile is derived *without* any additional fitting parameter. The other considered profile is interdiffusion with a uniform diffusion coefficient. Though this mechanism is reported to be less important than segregation in typical CdTe QW's, the situation turns out to be different for the structures studied embedded within an optical cavity. For the latter, the comparatively long DBR deposition periods lead to sizable interface diffusion. A combination of *error functions* (erf) has been used to model the interdiffusion induced compositional profile $X(z)$ of the QW's (Ref. 6):

$$X(z) = 0.6\left(1 - \frac{1}{2}\,\mathrm{erf}\left[\frac{z+\frac{3d_1}{2}+d_2}{d_0}\right] + \frac{1}{2}\,\mathrm{erf}\left[\frac{z+\frac{d_1}{2}+d_2}{d_0}\right] - \frac{1}{2}\,\mathrm{erf}\left[\frac{z+\frac{d_1}{2}}{d_0}\right] + \frac{1}{2}\,\mathrm{erf}\left[\frac{z-\frac{d_1}{2}}{d_0}\right] - \frac{1}{2}\,\mathrm{erf}\left[\frac{z-\frac{d_1}{2}-d_2}{d_0}\right] + \frac{1}{2}\,\mathrm{erf}\left[\frac{z-\frac{3d_1}{2}-d_2}{d_0}\right]\right). \quad (6)$$

d_1 and d_2 indicate the nominal widths of the CdTe (X=0) and $Cd_{0.4}Mg_{0.6}Te$ (X=0.6) layers, respectively, and d_0 is the transition width. Figure 6 shows, with the thicker symmetric curve, a sketch of the profile of one of the three QW's. The shadowed area of width $2d_0$ defines the interface region from 8% to 92% of the maximum Mg concentration (i.e., from X=0.047 to X=0.553). Note that for $d_0\to 0$, since erf(z) tends to a Heaviside function (step function), the structure approaches three perfect squared wells. For the interdiffusion model, Eq. (5) was solved recursively, changing the compositional profile through the parameter d_0, and changing ω_0 to fit the frequency of the LO_2 peak. On the other hand, for the segregation case the compositional profile is fixed by the model, and only $\omega_0$was changed to adjust the LO_2 peak's position.

The calculated phonon dispersion derived assuming an exponential-like segregation profile is shown in Fig. 5 (triangles). It is evident from this calculation that segregation alone cannot explain the observed equidistance between confined optical phonon modes. In fact, though the phonon dispersion is flattened respect to the bulk, it maintains a quadraticlike behavior markedly different from the almost linear dependence observed in the experiments. The latter, on the other hand, can be well accounted for when the more paraboliclike interdiffusion profile is assumed. Best fits were achieved for ω_0=173.8 cm^{-1} and d_0=11 Å. The calculated phonon dispersion is shown in Fig. 5 with small dots, and the solid line is an interpolation between the corresponding calculated points. These results are relatively stable (within 0.02% and 1%, respectively) for variations of 7% of the parameters α and β_0. One point worth mentioning is that the QW barriers of the phonon potential are high enough for the confined phonons of the three QW's to be uncoupled and degenerate. Thus, modeling the system with only one QW inside the cavity gives identical results.

The obtained phonon confining potential evidences a relatively strong rounding of the ideally square QW potential. In fact, the value derived for d_0 corresponds to a total interface width ($2d_0\sim 2$ nm) of about 14 atomic layers, while the nominal QW thickness amounts to 44 atomic layers. In fact, previous studies indicate that cation atomic diffusion mobilities in CdTe are high. This is partially explained by the fact that Mg is 5 times lighter than Cd and Te. We note that, although the MBE growth temperature used was relatively low (~300 °C), the time required to deposit the top Bragg reflector of the microcavity is large (~3 hours), further con-

tributing to the potential rounding. Based on the published diffusivity of Mg in CdTe,[18] we have estimated a diffusion length of ~1.5 nm, which agrees well with the phonon potential shape derived from our Raman data. On the other hand, the fitted frequency ω_0 is slightly larger ($\lesssim 3$ cm^{-1}) than the "bulk" value found in the literature.[26,27] This fact might indicate the presence of some uniform strain throughout the well structure,[25,28] something probably related with the altered compositional profile.

Very few papers have addressed, to the best of our knowledge, the Raman scattering due to confined optical phonons in single or few QW's.[29] The reason for this relies on the fact that the cross section for these scattering processes is relatively low. Most of the research on confined vibrations and the knowledge derived from this research have dealt with superlattices based on III-V materials. In fact, there is only a small number of reports dealing with confined vibrations in superlattices grown from II-VI materials and phonon dispersions derived from this QW confinement.[28,30–32] The relative poorer sample quality of II-VI QW's (as compared to, e.g., GaAs/AlAs) has probably hampered the observation of the rich related phenomena studied in III-V materials. We have thus approached this problem using a strategy based on Raman amplification in optical microcavities. In fact, it has been demonstrated that Raman scattering is strongly enhanced by embedding the structure studied within a semiconductor microcavity.[33–35] The strong photon confinement and consequent enhancement of the electric field at the cavity spacer leads to an amplification of the Raman cross section on the order of 10^4-10^5. In addition, when the scattering process is tuned at resonance with "real" electronic transitions the Raman cross-section enhancement can be further increased.[2,36] In the experiments reported here, the middle polariton to which the resonant Raman scattering is tuned is a mixed state of strongly enhanced electric field and QW-confined excitons. Thus, both effects, cavity and exciton resonant enhancement, are present. As previously demonstrated,[19,20] the Raman scattering process in the photon-exciton strong-coupling regime is amplified, on top of the pure electromagnetic factor, by at least two orders of magnitude, leading to efficiency improvements in the range 10^6-10^7. This strong amplification explains the clear observation of confined vibrations in the studied structure with only three CdTe QW's.

V. CONCLUSIONS

In summary, we have reported the experimental observation of polariton-mediated outgoing resonant Raman scattering due to confined longitudinal optical phonons of three CdTe quantum wells embedded in a II-VI-type semiconductor microcavity. The Raman line shape in the optical phonon region, corresponding to the confined phonons, consists of a main peak plus a series of equidistant oscillations towards lower Raman shifts. Using an effective-mass model and based on the effective dispersion of the observed Raman modes, we have proven that it is possible to derive and estimate with good accuracy the compositional profile of the quantum wells. Our experimental results together with the obtained profiles indicate the existence of interdiffusion in addition to segregation at the interfaces and the possible presence of uniform strain throughout the well structure. Segregation, interdiffusion, and strain are responsible for providing the elastic-scattering mechanism required for the observation of the Fröhlich-interaction-mediated vibrations with finite $q_\parallel$.

ACKNOWLEDGMENTS

We deeply acknowledge Jean Marie Moison for providing the simulation code used to evaluate the segregation profile. Support from SECyT-ECOS is also acknowledged.

*Electronic address: bruchhau@cab.cnea.gov.ar
†Also at CONICET, Argentina. Electronic address: afains@cab.cnea.gov.ar

[1] For a tutorial review, see B. Jusserand and M. Cardona, in *Light Scattering in Solids V*, edited by M. Cardona and G. Güntherodt (Springer-Verlag, Berlin, 1989), and references therein.
[2] J. Menéndez, J. Lumin. **44**, 285 (1989).
[3] M. Babiker, J. Phys. C **19**, 683 (1986), and references therein.
[4] R. Pérez-Alvarez, F. García-Moliner, V. R. Velasco, and C. Trallero-Giner, J. Phys.: Condens. Matter **5**, 5389 (1993). and references therein.
[5] M. P. Chamberlain, M. Cardona, and B. K. Ridley, Phys. Rev. B **48**, 14356 (1993), and references therein.
[6] B. Jusserand, F. Alexandre, and G. L. Roux, Appl. Phys. Lett. **47**, 301 (1985).
[7] B. Jusserand, F. Mollot, J. Moison, and G. L. Roux, Appl. Phys. Lett. **57**, 560 (1990).
[8] A. K. Sood, J. Menéndez, M. Cardona, and K. Ploog, Phys. Rev. Lett. **54**, 2111 (1985).
[9] A. K. Sood, J. Menéndez, M. Cardona, and K. Ploog, Phys. Rev. Lett. **54**, 2115 (1985).
[10] A. J. Shields, M. Cardona, and K. Eberl, Phys. Rev. Lett. **72**, 412 (1994).
[11] A. J. Shields, M. P. Chamberlain, M. Cardona, and K. Eberl, Phys. Rev. B **51**, 17728 (1995).
[12] J. M. Moison, F. Houzay, F. Barthe, J. M. Gérard, B. Jusserand, J. Massies, and F. S. Turco-Sandroff, J. Cryst. Growth **111**, 141 (1991).
[13] D. Levi, S.-L. Zhang, M. V. Klein, J. Klem, and H. Morkoç, Phys. Rev. B **36**, 8032 (1987).
[14] G. S. Spencer, J. Menéndez, L. N. Pfeiffer, and K. W. West, Phys. Rev. B **52**, 8205 (1995).
[15] J. M. Moison, C. Guille, F. Houzay, F. Barthe, and M. Van Rompay, Phys. Rev. B **40**, 6149 (1989).
[16] W. Grieshaber, J. Cibert, J. A. Gaj, Y. Merle d'Aubigné, and A. Wasiela, Phys. Rev. B **50**, 2011 (1994).
[17] W. Grieshaber, A. Haury, J. Cibert, Y. M. d'Aubigné, A. Wasiela, and J. A. Gaj, Phys. Rev. B **53**, 4891 (1996).

[18] A. Seweryn, T. Wojtowicz, G. Karczeski, A. Barcz, and R. Jakiela, Thin Solid Films **367**, 220 (2000).
[19] A. Fainstein, B. Jusserand, and V. Thierry-Mieg, Phys. Rev. Lett. **78**, 1576 (1997), and references therein.
[20] A. Fainstein, B. Jusserand, and R. André, Phys. Rev. B **57**, R9439 (1998), and references therein.
[21] A. Bruchhausen, A. Fainstein, B. Jusserand, and R. André, Phys. Rev. B **68**, 205326 (2003).
[22] G. Fasol, M. Tanaka, H. Sakaki, and Y. Horikoshi, Phys. Rev. B **38**, 6056 (1988).
[23] P. Y. Yu and M. Cardona, *Fundamentals of Semiconductors: Physics and Material Properties* (Springer-Verlag, Berlin, 1996).
[24] E. Oh, C. Parks, I. Miotkowski, M. D. Sciacca, A. J. Mayur, and A. K. Ramdas, Phys. Rev. B **48**, 15040 (1993).
[25] V. C. Stergiou, N. T. Pelekanos, and Y. S. Raptis, Phys. Rev. B **67**, 165304 (2003), and references therein.
[26] J. M. Rowe, R. M. Nicklow, D. L. Price, and K. Zanio, Phys. Rev. B **10**, 671 (1974).
[27] D. J. Olego, P. M. Raccah, and J. P. Faurie, Phys. Rev. B **33**, 3819 (1986).
[28] J. Menéndez, A. Pinczuk, L. Valladares, R. D. Feldman, and R. F. Austin, Appl. Phys. Lett. **50**, 1101 (1987).
[29] A. K. Arora, E. K. Suh, A. K. Ramdas, F. A. Chambers, and A. L. Moretti, Phys. Rev. B **36**, 6142 (1987).
[30] E.-K. Suh, D. U. Bartholomew, A. K. Ramdas, S. Rodriguez, S. Venugopalan, L. A. Kolodziejski, and R. L. Gunshor, Phys. Rev. B **36**, 4316 (1987).
[31] E. Oh, A. K. Ramdas, T. Fromherz, W. Faschinger, G. Bauer, and H. Sitter, Phys. Rev. B **48**, 17364 (1993).
[32] T. Fromherz, F. Hauzenberger, W. Faschinger, M. Helm, P. Juza, H. Sitter, and G. Bauer, Phys. Rev. B **47**, 1998 (1993).
[33] A. Fainstein, B. Jusserand, and V. Thierry-Mieg, Phys. Rev. Lett. **75**, 3764 (1995).
[34] A. Fainstein, B. Jusserand, and V. Thierry-Mieg, Phys. Rev. B **53**, R13287 (1996).
[35] A. Fainstein and B. Jusserand, Phys. Rev. B **57**, 2402 (1998).
[36] R. M. Martin and L. M. Falicov, in *Light Scattering in Solids I*, edited by M. Cardona (Springer-Verlag, Berlin, 1989), and references therein.
[37] Note that for energies above ~1.6525 eV the experimental points of $\Delta\omega$ fall slightly below the mean value (indicated by the solid line in Fig. 4). This is probably an artifact related to the determination of the oscillations position as the peak maxima. As shown in Fig. 2 in resonant conditions the oscillations move on top of the medium polariton peak. Thus, the existence of an inclined background may explain this subtle feature.